City Research Online

City, University of London Institutional Repository

Novel 3D-printed biaxial tilt sensor based on fiber Bragg grating sensing approach

N.N. Ismail [a], A.S. Sharbirin [a], M.S.M. Sa'ad [a], M.K.A Zaini [a], M.F. Ismail [a,*], G. Brambilla [c],
B.M.A. Rahman [b], K.T.V. Grattan [b], H. Ahmad [a,d]

[a] *Photonics Research Center, University of Malaya, 50603, Kuala Lumpur, Malaysia*
[b] *School of Mathematics, Computer Science and Engineering, City, University of London, London, EC1V 0HB, United Kingdom*
[c] *Optoelectronics Research Centre, University of Southampton, Southampton, SO17 1BJ, United Kingdom*
[d] *Physics Dept. Faculty of Science, University of Malaya, 50603, Kuala Lumpur, Malaysia*

A B S T R A C T

In this work, a novel 3D-printed biaxial sensor system for tilt measurement, based primarily on the use of four Fiber Bragg Grating (FBG) devices, has been developed and its performance characterized. The tilt sensor system created is of a compact design and relatively small dimensions, making it ideally suited to a variety of industrial applications. In the system developed, the four FBGs used were spliced in a serial formation and attached to four different sides of the sensor structure designed, to allow biaxial measurements to be made. The wavelengths' shift of the FBGs used were monitored as a function of the tilt of the device, using an Optical Spectrum Analyzer (OSA) for this development work. In the sensor, an average FBG-based responsivity of 0.01 nm/$^\circ$ of tilt was measured for each of the different FBGs used. To provide compensation for temperature changes in the system itself, a further FBG-based approach was used (in which they were configured to be insensitive to the effect of the tilt). They were thus calibrated by being exposed to a range of operational temperatures for the system, showing, as a result, a calibration of 0.011 nm/$^\circ$C. Prior work on the sensor system had proved it to be highly linear in response, over the tilt range of $0^\circ \pm 90^\circ$. The experimental results obtained from the performance characterization indicate that the small, compact design of this type yields excellent responsivity, compared to other larger and more complex designs discussed in the literature. The sensor system was also relatively easy to fabricate using the 3D-printing method, creating in that way an inexpensive, temperature-compensated tilt monitoring device that had a wide variety of potential industrial applications.

1. Introduction

Tilt sensors are very important for the measurements of angular deviation of a structure, with respect to a fixed reference plane, for a number of applications in the industry. Sensors of this type can be found, for example, in the field of aviation to monitor the aircraft angle tilt and most frequently in civil and structural engineering, where typically the need is to monitor the inclination of buildings [1] or bridges [2]. There are also Electromyography (EMG) based sensors that study the human-computer interaction [3] and force predictions in the human body [4,5]. A further important application in geotechnical engineering is in the use of tilt sensors for the measurement of ground movements that can occur

for a variety of different reasons, such as due to earthquakes, and landslides which can be caused in earth structures due to heavy rainfall, for example [6–8]. Most of the existing tilt sensors that have been designed are comprise of relatively larger mechanical parts and more complicated electronic components. For instance, even though mechanical-based tilt sensors such as vertical and horizontal gravitational pendulum sensors are stable, the measurement can only be obtained by manual observation on the instrument pointer where there are no electrical signals available for post-processing. Therefore, the use of the sensor requires manual and well-trained observers. Furthermore, adding electronic circuitries to the mechanical sensors to acquire the measurement data will complicate the hardware, which in the end will increase the production and maintenance cost. On the other hand, the existing electronic-based tilt sensors are mostly functioning based on either a magnetic [9] or capacitive effect [10]. Even though their sensitivity is good, they can be affected by a short circuit which is caused

by water or moisture in wet environment conditions. Furthermore, electronic-based sensors are susceptible to electromagnetic interference, which can be an issue in some field or on-site applications. The latest sensors [11,12] also seem to be easily affected by buoyancy forces. Most of the existing tilt sensors experienced torsion and buoyancy forces caused by the liquid filler at the time it was inserted to fill the gap between the sensors and its casing during installation, which causes inaccurate measurements [13]. Hence, spiral checks, manual inspections, and time-consuming corrections in the output data are required [14,15]. This additional requirement is causing the system to be more complicated to handle and bulky. Thus, to overcome these problems, a new non-electrical-based design is proposed in this work.

A Fiber Bragg Grating (FBG)-based approach has been introduced to create this novel tilt sensor design, taking advantage of the special features that this technology shows over the use of electronic-based sensors for applications like this. FBG-based devices take advantage of immunity to electromagnetic interference, electrically passive operation, and multiplexing capabilities [16,17]. In general, the FBG sensor operates by detecting strain and temperature resulting from the shift in the reflected wavelength observed: hence, this technology is inherently independent of any twist or rotation to the sensor and this offers a solution to twist errors seen with conventional sensors. In previously reported work as in the literature, various designs of FBG-based tilt sensors have been developed [18–21]. However, most of this research is on uniaxial detection [19]: thus, a combination of two sensors is required to detect the change along two translational axes i.e. the x- and y-axis. As an example, in the case of the biaxial tilt sensor proposed by Kai Ni et al. [20] which utilizes four FBGs, designed as a pendulum structure where each FBG detects the tilt angle along a different axis. X. Dong et al. [21], Bao et al. [22], Au et al. [23] and S. He et al. [24] have also demonstrated a biaxial temperature-insensitive tilt sensor with a hanging pendulum structure. However, the major disadvantage here is that this introduces unwanted mechanical friction, rotations, and instabilities in the measurement. Several tilt sensors such as reported by Xu et al. [25] and Hong et al. [26] have designed the tilt sensor based on the pendulum system with central support where the dead weight was mounted to the shaft of the sensor. However, both designs only cover uniaxial measurements as it consists only 2 FBGs, left and right. In reference [27], the authors used an array FBG covering 2 sides of a beam. The drawback of this design is that the tilted angle was measured when there is a slope deformation, which caused damage to the sensor. In an effort to overcome the limitations seen with previous work, both non-optical and optically based, in this paper, the design and performance evaluation of a new sensor design incorporating four FBGs with different reflective wavelengths, attached to four different sides of the overall sensor structure (representing the x and y-axis) is presented. The fused deposition modeling (FDM) method used in this work can create highly precise sensor components with a fine resolution of 0.01-inch thickness by the 3D printer. Thus, any desired sensor components can be accurately fabricated, and this proposed approach has overcome the limitations of traditional manufacturing methods. Besides, the four FBGs attached to the design provide high sensitivity to the tilt angle change in biaxial measurements. The tilt sensor developed is compact in size (of length only 7.1 cm), yet sturdy in the configuration as compared to other FBG-based sensors, to suit it for use in many demanding civil and structural monitoring applications. The sensor operates over a tilt range from -90° to +90°, in both the x and y-axis, where the associated FBG-based wavelength shifts are observed and recorded using an Optical Spectrum Analyzer (OSA), and calibrated against known, measured tilts in the laboratory. Further, temperature compensation using a further tilt-insensitive FBG system is in-built, to allow the device to be used in a wide variety of situations, including where the temperature fluctuates.

2. Fabrication and working principle of the FBG-based system

The FBGs used in this work were fabricated using the phase mask technique by inscribing uniform FBGs in the core of standard SMF. Prior to the FBG fabrication process, the SMF was soaked in a high-pressure hydrogen tube (~2000 psi) for 5 days to photosensitize the fiber. Then, pulses from a Krypton Fluoride (KrF*) excimer laser (at a wavelength of 248 nm) were used to inscribe 10 mm gratings inside the fiber core. After the fabrication process was complete, the SMF samples containing the FBGs were annealed in an oven at temperatures ~70−80 °C for 7 h, to eliminate the residual hydrogen.

For an FBG written in a single-mode fiber, the Bragg wavelength shift is associated with the strain, ε and temperature, T change, can be described as:

$$\frac{\Delta\lambda_B}{\lambda_B} = (1 - p_{eff})\Delta\varepsilon + (\alpha + \xi)\Delta T \qquad (1)$$

where λ_B is the Bragg wavelength, p_{eff} is the photo-elastic parameter, α is the thermal expansion coefficient and ξ is the thermo-optic coefficient of the fiber.

3. Sensor design and structure and measurement setup

3.1. Tilt sensor design

The illustration of the FBG tilt sensor system, in this case, set at an inclination angle, θ, is shown in Fig. 1(a). The overall tilt sensor design developed in this work is shown schematically in Fig. 1(b) at inclination angle, θ, equal to zero, where the dimensions of the conveniently 3D-printed device are based on a shaft length of 4 cm. This sensor is fabricated purely by using a 3D printer with polylactic acid (PLA) as its source material. The PLA is one of the most common materials used in 3D printing nowadays hence making the sensor easy to be fabricated. As can be seen from the diagram, the top section of the sensor is a cube with a dimension of 1.2 × 1.2 × 1.2 cm, while the bottom section has dimensions of 1.9 × 1.2 × 1.2 cm. A schematic of the way the tilt sensor discussed is used in practice can be seen in Fig. 1(c), illustrating that it is based on a vertical pendulum structure. Four different FBGs (shown as FBG 1 to FBG 4), with reflective wavelengths of 1534.1 nm, 1544.2 nm, 1551.1 nm, and 1558.3 nm respectively were incorporated into the tilt sensor to represent two translational axes, as shown schematically in Fig. 1(d). A ~1550 nm amplified spontaneous emission (ASE) input light source was connected to port-1 of the 4-port optical circulator shown and the response of the FBG tilt sensor system was observed using a Yokogawa AQ6370C 600–1700 nm OSA, which was connected to port-3 of the circulator.

As illustrated in Fig. 1(e), in the setup used to evaluate and calibrate the sensor, a 5 g metallic deadweight was attached to each side of the bottom section of the sensor device (a total of four metallic weight, 20 g) to induce strain to the FBG during tilting. As illustrated in the diagram, the device was constructed so that an FBG was positioned on each side of the 3D printed sensor, through four holes that were design-printed on the sensor, to allow evaluation on both the positive and negative directions of the x and y-axis. The FBGs were pre-stressed through a procedure carried out by pulling the end of each FBG, before being glued using strong liquid adhesive (Super Glue, cyanoacrylate) at each end in order to ensure the integrity of each FBG used, FBG 1 to FBG 4. The FBGs were pre-stretched until they were at a strained-tight position. At 0° tilt (initial position), the wavelength spectrum is considered as
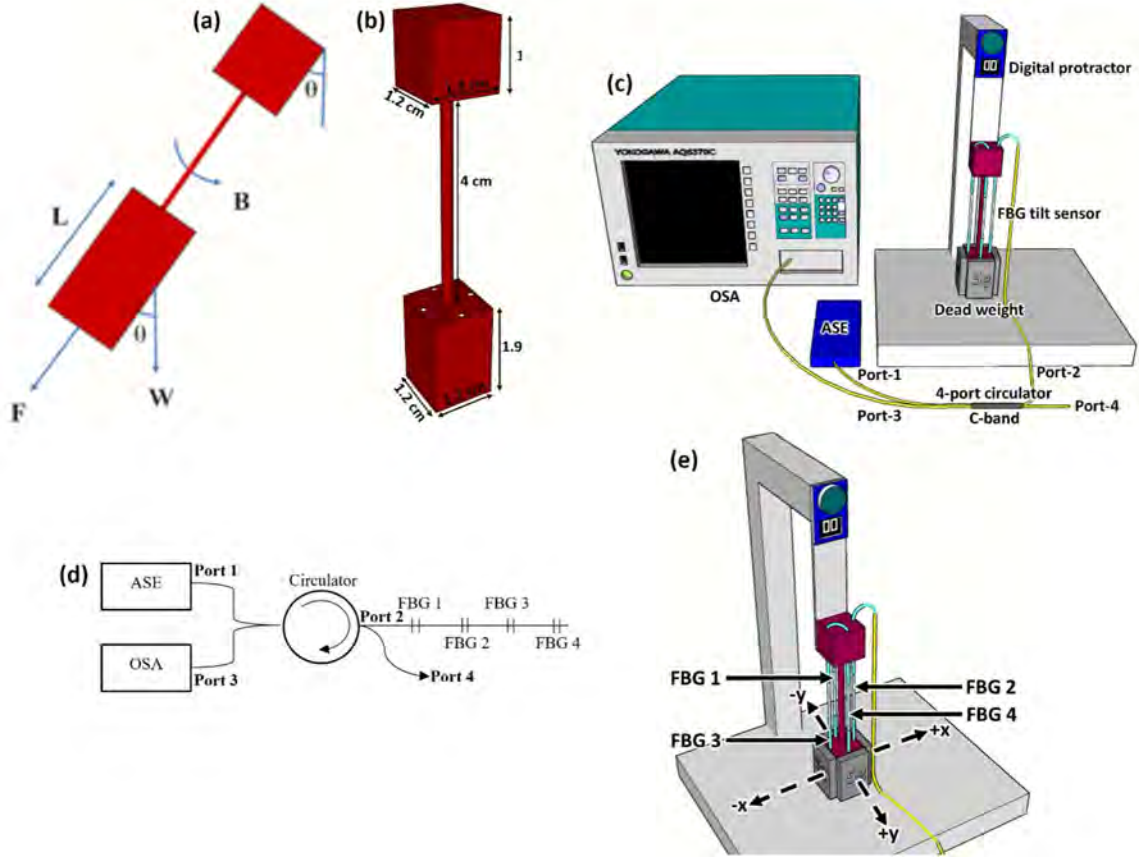
Fig. 1. Illustrations of (a) FBG tilt sensor at an inclination angle, θ, (b) the tilt sensor dimensions when upright i.e. $\theta = 0$, (c) the FBG-based tilt sensor in the test and evaluation environment with the OSA used, (d) schematic of the FBG-based (FBG 1 to FBG 4) interrogation system employed (where ASE is the optical source and OSA is the optical spectrum analyzer (seen also in (c)); and (e) shows the set up for the evaluation of the tilt sensor calibration and the positions of the four FBGs on the basic 3-D printed sensor (from (b)) with the coordinate axis.

the initial spectrum. The FBGs were then spliced in a serial configuration and connected to port-2 of the optical circulator. To evaluate its performance, the tilt sensor was then mounted on a digital protractor where it was calibrated by varying the tilt angle towards inclination axes (+x, -x, +y, -y). The direction of movement of the tilt sensor and the positions of each of the FBG-based tilt sensors used are shown in Fig. 1(e), where FBG 2 was placed on the positive x-axis, FBG 3 on the negative x-axis, FBG 4 on the positive y-axis and FBG 1 on the negative y-axis. When the tilt sensor was moved in the positive x-axis direction, FBG 2 would be stretched while FBG 3 would be compressed, and *vice versa*, while FBG 1 and FBG 4 remain unchanged. The same method was used to measure the effects on FBG 1 and 4 in the y-axis direction. During the calibration, the tilt sensor was tilted towards inclination axes over the range from 0° to 90°, in 10° intervals.

As FBGs are very fragile, we placed the tilt sensor in a 12cm × 7.5cm x 4.8 cm 3D-printed rectangular cover in order to protect the FBGs during calibration. The cover was printed separately as two parts and was glued together with the sensor in the middle. The exact dimension of the cover is illustrated in Fig. 2(a) while the actual pictures of the printed cover with the tilt sensor are depicted in Fig. 2(b).

The Bragg wavelength shifts of the four FBGs can then be used to determine the tilt angle magnitudes. The tensile force, F_T and bend moment, B of the sensor can be described in terms of the tilt angle as follows:
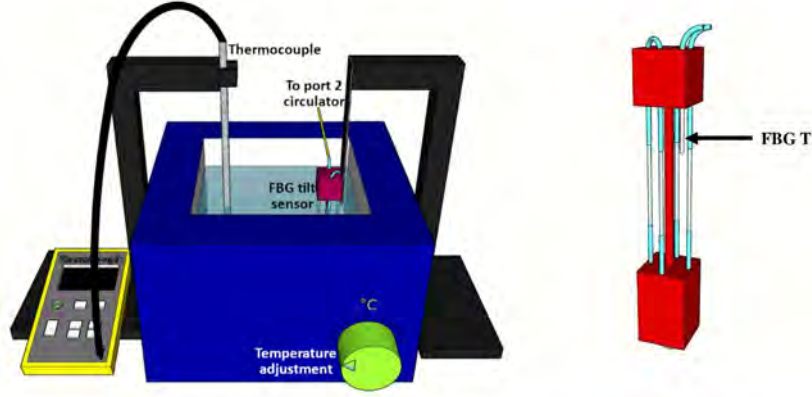
$$F_T = W \cos\theta \tag{2}$$

$$B = W \cdot L \sin\theta \tag{3}$$
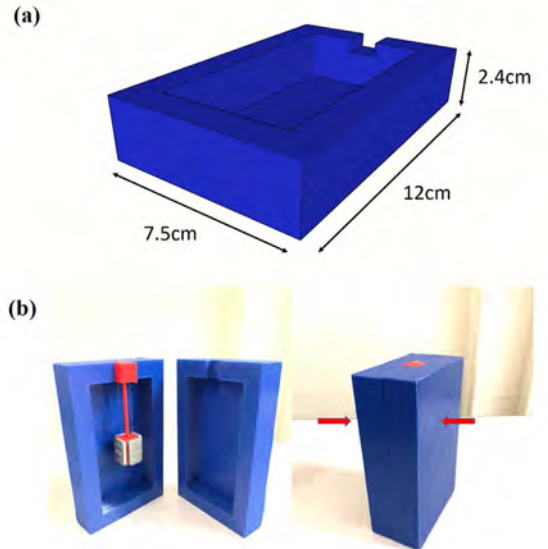
Fig. 2. (a) the dimensions of the 3D-printed cover and (b) the actual pictures of the cover with the tilt sensor.

where W is the dead weight and L is the length of the dead weight. Both tensile force and bending moment cause strain change to the four FBGs and this change can be derived by:

Fig. 3. Illustration of (a) the temperature compensation experiment using a water bath setup in which the sensor system is immersed, (b) tilt sensor design with FBG T left hanging.

$$\varepsilon = \frac{F_T}{EA_s} \pm \frac{B}{EI_s} \tag{4}$$

where E, A, and I_s are the elastic modulus, cross-sectional area, and moment of inertia of the sensor shaft, respectively. Based on Eq. (2) and (3), the strain change due to inclination angle can be calculated from:

$$\varepsilon = \frac{F_T}{EA_s} \pm \frac{B}{EI_s} = \frac{W}{E}\left(\frac{\cos\theta}{A_s} \pm \frac{L\sin\theta}{I_s}\right). \tag{5}$$

3.2. Temperature compensation

The system had been designed with integral temperature compensation and to evaluate, a series of measurements were carried out in a water bath, as illustrated in Fig. 3(a). Initially, the FBGs need to be characterized for their response due to temperature changes. To do so, the temperature of the water bath was gradually increased while, at the same time, the wavelength shifts of each of the FBGs, FBG 1–4 was observed and calibration data were measured and recorded. To undertake a full calibration of the tilt sensor system, a thermocouple was used to monitor the water temperature and the device was submerged into the water bath, placed vertically at the 0° position. The temperature was increased gradually (in 10 °C intervals) over the range from room temperature (27 °C) to 80 °C. The procedure was repeated with another FBG added (denoted as FBG T) to this design as shown in Fig. 3(b), to act as a temperature sensor to monitor temperature changes surrounding the inclinometer. The FBG was left hanging to ensure strain insensitivity. This further illustrates that the sensor system can be used when wet or fully immersed, as would be the case in measurements of earth movements during heavy rainfall or flooding when the temperature also can vary widely.

4. Results and discussion

As discussed above, four FBGs (FBG 1–4) with distinct wavelength peaks were used to measure the angular deviations at the two axes. The FBG base wavelength characteristics and their respective axis are as given in Table 1.

Fig. 4(a) shows the base reflected peaks produced from the four FBGs, FBG 1–4, that form the tilt sensor and before the sensor is tilted. As the sensor is then tilted towards the -y direction, a shift in the spectrum can be observed as shown in Fig. 4(b), where it is evident that the signal on FBG 1 (negative y-axis) shifts to longer wavelengths ('redshifts'), indicating a tension acting on the fiber. The figure shows clearly that the other signals do not show any observable changes, illustrating that the sensor is working as

Table 1
FBGs with their assigned base wavelengths (at room temperature of 27 °C) and associated axis.

| FBG #	Base Wavelength	Axis
1	1534.1	-y
2	1544.2	+x
3	1551.1	-x
4	1558.3	+y
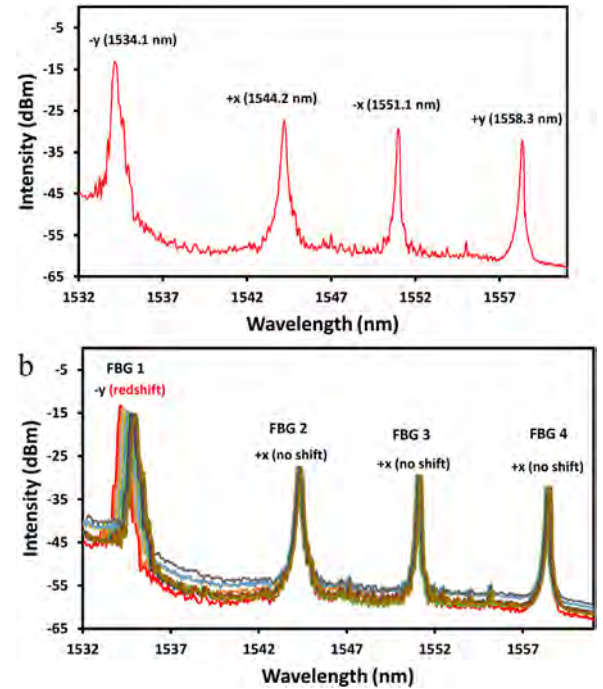
Fig. 4. a) Four base wavelength peaks of FBG 1 to 4 (see Table 1) from the tilt sensor (at room temperature of 27 °C), before the sensor was tilted. **b)** Shift in the wavelength spectrum of FBG 1 to 4 (see Table 1, at room temperature of 27 °C) after the sensor was tilted towards the -y direction.

intended – it clearly shows a localized tilt depending on the axis of direction i.e. the negative y-axis. Fig. 5(a) shows the noticeable change in the wavelength of the signal with an increase in tilt in greater detail, reflected in the redshifted peak on the y-axis over the range from 0° → -90°. The experiment was repeated using similar shifts along the remaining axes (+x, -x, and + y), where the respective spectra for each from 0° → 90° were recorded and shown in Fig. 5(b), (c), and (d).
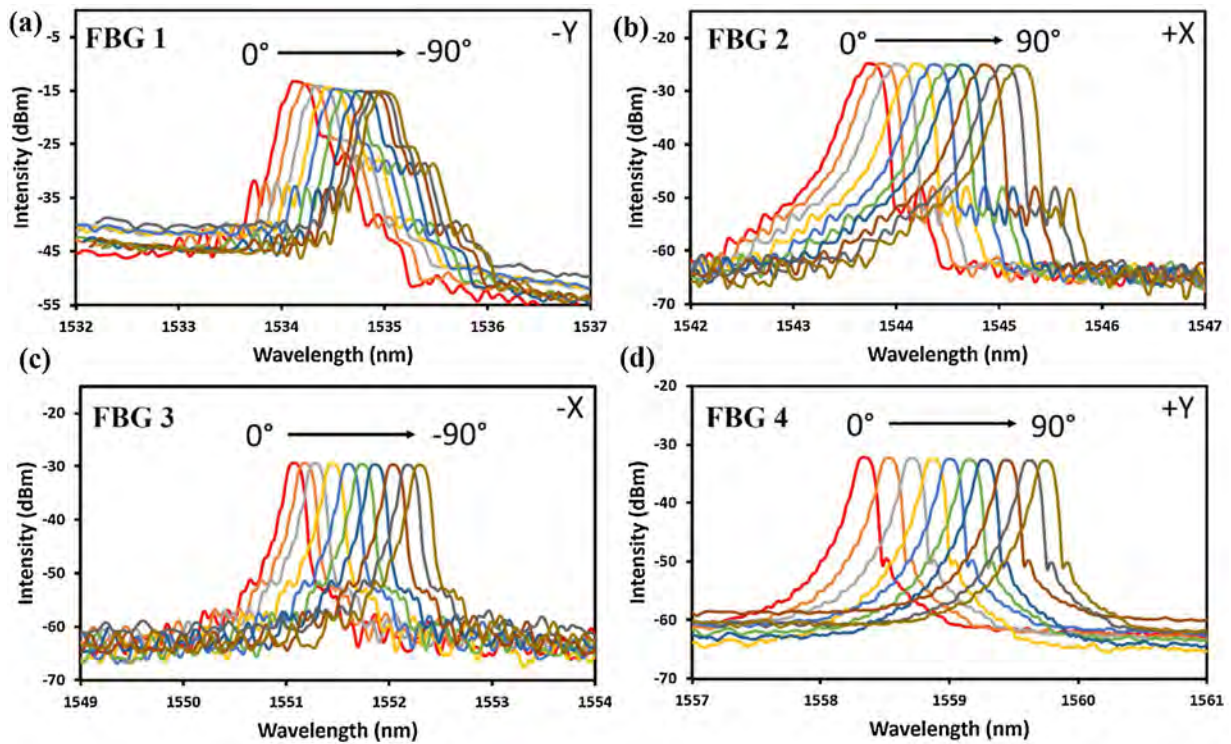
Fig. 5. Spectrum of the wavelength shifts ('redshift') from 0° → 90° (a) FBG 1 towards the negative angle on the y-axis, (b) FBG 2 towards the positive angle on the x-axis, (c) FBG 3 towards the negative angle on the x-axis, and (d) FBG 4 towards the positive angle on the y-axis. Measurements were carried out at room temperature of 27 °C.
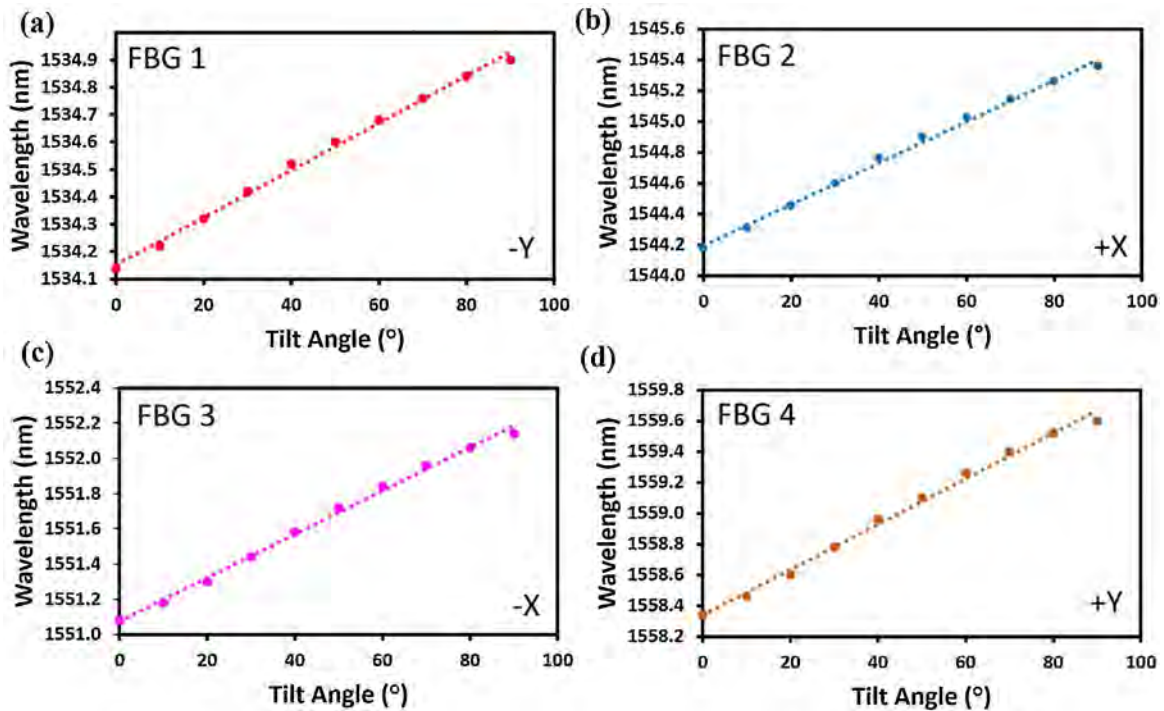
Fig. 6. Wavelength response in the sensor system over the tilt angle from 0° → 90° (a) FBG 1 on the negative y-axis, (b) FBG 2 on the positive x-axis, (c) FBG 3 on the negative x-axis, and (d) FBG 4 on the positive y-axis. Measurements were carried out at room temperature of 27 °C.

Based on the measurements from the sensor system, illustrated in Fig. 5(a), (b), (c), and (d), the relationship between the signal wavelength and the tilt angle has been plotted to show the responsivity of the sensor. The wavelength to tilt relationship thus obtained is shown in Fig. 6(a), (b), (c), and (d), illustrating that all the FBGs show a linear relationship with the tilt angle, up to 90°.

It is clear that the sensor shows an excellent linear response over the range between -90° to +90° for both axes, and which makes the sensor system very well suited to a range of important applications in various industries.

Table 2 summarizes the results derived from Fig. 6(a)–(d), showing the responsivity of each FBG (FBG 1–4) with tilt angle,
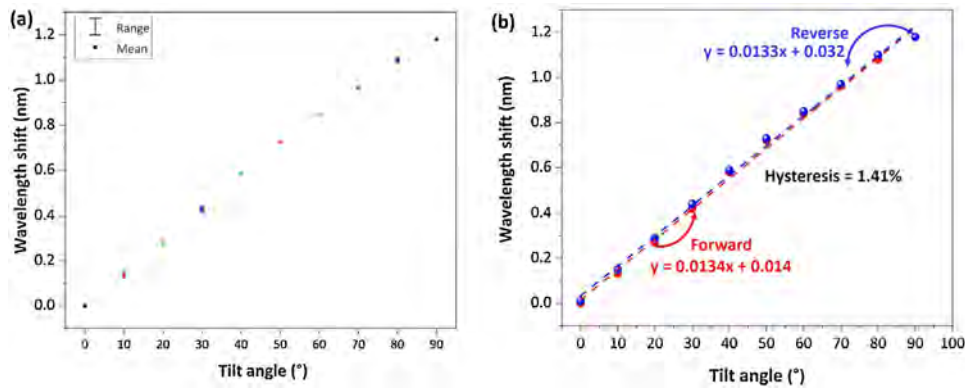
Fig. 7. Repeatability test of the sensor system (a) interval plot between 6 data and (b) hysteresis characteristic.

Table 2
FBGs (FBG 1 – 4) with their assigned axis and responsivity towards the tilt angle used. Measurements were carried out at room temperature of 27 °C.

FBG #	Axis	Responsivity (nm/°)	R^2
1	-y	0.009	0.9962
2	+x	0.013	0.9966
3	-x	0.012	0.9961
4	+y	0.015	0.9945

illustrating the respective R^2 values of the linear part of the fit. The responsivity of each installed FBG in the sensor system is different and distinctive, each being strongly affected by the level of pre-stress applied to the fiber, as it is fitted to the sensor body. A higher level of pre-stress will result in a bigger shift in the wavelength with each variation of the tilt angle. Therefore, the flexibility of the design of the sensor system allows its configuration to be tailored for different applications, so that for those which require the detection of small-angle deviations (« 1°), a stronger pre-stress can be applied. However, doing so increases the risk of the fiber breaking, at larger values of the tilt angle.

To evaluate the repeatability of the sensor system, the response between the tilt angle and the wavelength shift has been measured and repeated 6 times, and the strain hysteresis profiling has been carried out to one of the axes which are on the positive x-axis (FBG 2). Fig. 7(a) shows the interval plot between the 6 data where it can be seen that the deviation is very small. While in Fig. 7(b), the strain hysteresis of the sensor system was determined to be 1.41 %. Therefore, based on the repeatability test, it can be said that the system is repeatable.

The effectiveness of the temperature compensation applied has been studied and Fig. 8(a) shows the reflected spectrum of the four tilt-monitoring FBGs used (FBG 1–4) as they were exposed to a range of different temperatures, while Fig. 8(b) illustrates the shifts in greater details for FBG 2 (+x direction) over the range from 27 °C → 80 °C. This is to initially characterize the FBGs as they were exposed to different temperatures. All the FBGs studied show noticeable shifts in their base wavelength, as all were exposed to the temperature range mentioned above, up to a maximum of 80°C which makes it well suited to a wide variety of industrial applications. Based on the measurements obtained above, graphs of wavelength shift as a function of temperature for FBG 1, 2, 3, and 4 were plotted (at a fixed zero angle of tilt) as shown in Fig. 9(a), (b), (c) and (d) respectively – all the graphs showing an excellent, linear trend of wavelength shifts as the temperature increased, with an average responsivity of 0.011 nm/°C: as summarized in Table 3.

Referring to the diagram illustrated in Fig. 10, another FBG (denoted as FBG T with a Bragg wavelength of 1553.26 nm) were added into the tilt sensor design (it was left hanging to ensure
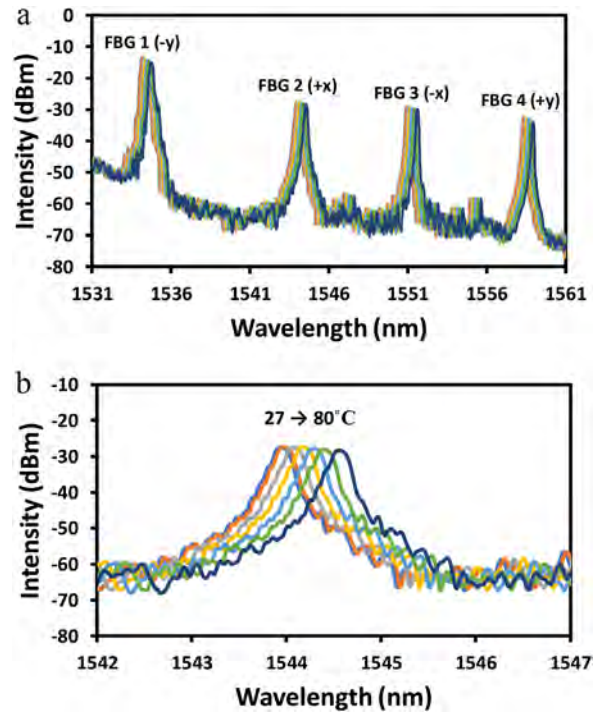

Fig. 8. a) Illustration of the temperature characterization in the sensor system: the shift in the wavelength spectrum of the FBGs (FBG 1 to 4) responding to their assigned axis, due to the applied changes in temperature over the range from 27°C → 80°C. **b)** Shift in the wavelength spectrum of a representative tilt-sensing FBG (in this case FBG 2), due to the change in temperature over the range from 27°C → 80°C.

Table 3
FBGs (FBG 1 to 4) with their assigned axis and responsivity to changes in temperature each at a fixed (zero) value of tilt.

FBG	Axis	Responsivity (nm/°C)	R^2
1	-y	0.010	0.9989
2	+x	0.011	0.9909
3	-x	0.012	0.9896
4	+y	0.011	0.9953

strain insensitivity), to act as a temperature sensor, allowing us to obtain a simple temperature compensation for this design. FBG T was also exposed to temperatures of 27°C to 80°C. The shifts in the wavelength spectrum and its linearity were shown in Fig. 10(a) and Fig. 10(b) respectively. A similar linear trend to those in Fig. 9 could be observed in Fig. 10(b) with a responsivity factor of 0.01 nm/°C along with the R^2 value that emphasizes the excellency of the fit.
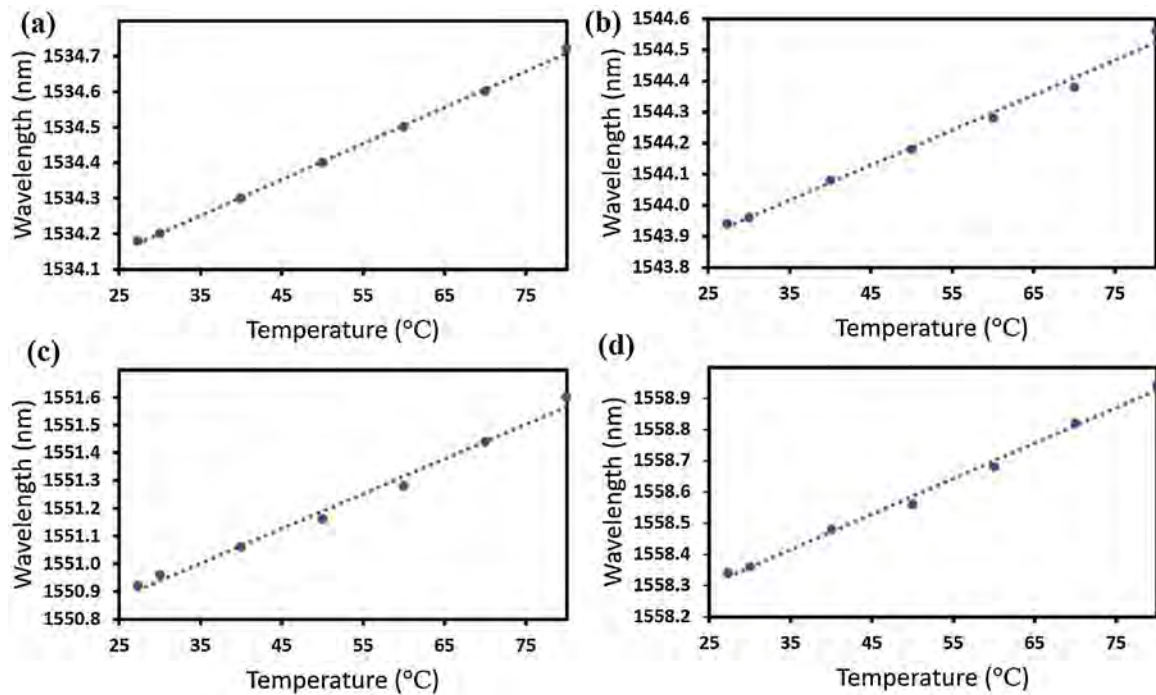
Fig. 9. Shift in the wavelength spectrum showing the linear response due to the change in temperature over the range from 27°C → 80°C (a) FBG 1, (b) FBG 2, (c) FBG 3, and (d) FBG 4, each at a fixed (zero) value of tilt.
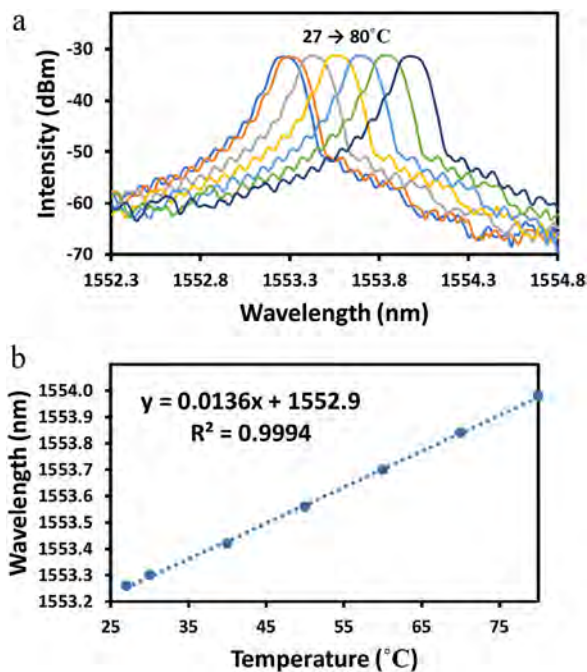
Fig. 10. a) Shift in the wavelength spectrum of FBG T, due to the change in temperature over the range from 27°C → 80°C. **b)** Shift in the wavelength spectrum showing the linear response due to the change in temperature over the range from 27°C → 80°C for FBG T, at a fixed (zero) value of tilt.

This proves a simple temperature compensation can be applied to the sensor system, to be used in a number of different applications.

5. Conclusions

A novel, simple and inexpensive, 3D-printed tilt sensor system has been designed and fabricated, to allow biaxial parameters to be measured in a temperature-compensated way, using a four-FBG based approach. The tilt sensor was designed and fabricated purely using a 3D printer with polylactic acid as its material, which is a common material used in 3D printing technology. Hence, the design is considered low cost and easy to fabricate as compared to conventional tilt sensors. Besides that, the sensor shows excellent linearity for each of the FBGs used, up to a tilt angle of 90°. An average maximum responsivity of about 0.01 nm/° per FBG over that range is reported, with a temperature compensation factor of 0.011 nm/°C which can be applied in the software. The experimental results indicate that this small, compact, and relatively easy-to-fabricate sensor design shows excellent responsivity, compared to other larger and complex designs reported in the literature. The ability to operate over a large angular range (up to ±90° on each axis), along with the compact design and flexibility in its fabrication, make this 3D-printed tilt sensor reported in this work, potentially widely applicable to a range of engineering systems on which important measurements can be made.

References

[1] T.H.T. Chan, L. Yu, H.Y. Tam, Y.Q. Ni, S.Y. Liu, W.H. Chung, L.K. Cheng, Fiber Bragg grating sensors for structural health monitoring of Tsing Ma bridge: background and experimental observation, Eng. Struct. 28 (2006) 648–659, http://dx.doi.org/10.1016/j.engstruct.2005.09.018.

[2] H.F. Lima, R. Da Silva Vicente, R.N. Nogueira, I. Abe, P.S. De Brito André, C. Fernandes, H. Rodrigues, H. Varum, H.J. Kalinowski, A. Costa, J. De Lemos Pinto, Structural health monitoring of the church of santa casa da misericórdia of Aveiro using FBG sensors, IEEE Sens. J. 8 (2008) 1236–1242, http://dx.doi.org/10.1109/JSEN.2008.926177.

[3] Y. Sun, C. Xu, G. Li, W. Xu, J. Kong, D. Jiang, B. Tao, D. Chen, Intelligent human computer interaction based on non redundant EMG signal, Alexandria Eng. J. 59 (2020) 1149–1157, http://dx.doi.org/10.1016/j.aej.2020.01.015.

[4] D. Jiang, G. Li, Y. Sun, J. Kong, B. Tao, D. Chen, Grip strength forecast and rehabilitative guidance based on adaptive neural fuzzy inference system using sEMG, Pers. Ubiquitous Comput. (2019), http://dx.doi.org/10.1007/s00779-019-01268-3.

[5] R. Ma, L. Zhang, G. Li, D. Jiang, S. Xu, D. Chen, Grasping force prediction based on sEMG signals, Alexandria Eng. J. 59 (2020) 1135–1147, http://dx.doi.org/10.1016/j.aej.2020.01.007.

[6] Y. Yoshida, Y. Kashiwai, E. Murakami, S. Ishida, N. Hashiguchi, Development of the monitoring system for slope deformations with fiber bragg grating arrays, in: D. Inaudi, E. Udd (Eds.), Smart Struct. Mater. 2002 Smart Sens. Technol. Meas. Syst., 2002, pp. 296–303, http://dx.doi.org/10.1117/12.472632.

[7] Y.-T. Ho, A.-B. Huang, J. Ma, B. Zhang, Ground movement monitoring using an optic fiber bragg grating sensored system 17th Int. Conf. Opt. Fibre Sensors., 5855, 2005, pp. 1020, http://dx.doi.org/10.1117/12.623596.

[8] C.Y. Hong, Y.F. Zhang, M.X. Zhang, L.M.G. Leung, L.Q. Liu, Application of FBG sensors for geotechnical health monitoring, a review of sensor design, implementation methods and packaging techniques, Sens. Actuators, A Phys. 244 (2016) 184–197, http://dx.doi.org/10.1016/j.sna.2016.04.033.

[9] R. Olaru, C. Cotae, Tilt sensor with magnetic liquid, Sens. Actuators, A Phys. 59 (1997) 133–135, http://dx.doi.org/10.1016/S0924-4247(97)80162-8.

[10] Inclinometers: Types, How They Work, & Functions, (n.d.). https://www.encardio.com/blog/inclinometer-types-how-it-works-uses/ (accessed January 7, 2021).

[11] O. Ozioko, H. Nassar, R. Dahiya, 3D printed interdigitated capacitor based tilt sensor, IEEE Sens. J. XX (2021), http://dx.doi.org/10.1109/jsen.2021.3058949, 1–1.

[12] S. Wang, Y. Wang, D. Liu, Z. Zhang, W. Li, C. Liu, T. Du, X. Xiao, L. Song, H. Pang, M. Xu, A robust and self-powered tilt sensor based on annular liquid-solid interfacing triboelectric nanogenerator for ship attitude sensing, Sens. Actuators, A Phys. 317 (2021) 112459, http://dx.doi.org/10.1016/j.sna.2020.112459.

[13] G. Machan, V.G. Bennett, Use of inclinometers for geotechnical instrumentation on transportation projects, Use Inclin. Geotech. Instrum. Transp. Proj. (2008), http://dx.doi.org/10.17226/23074.

[14] Inclinometer | cep-singapore, (n.d.). https://www.cep.com.sg/inclinometer (accessed December 16, 2020).

[15] Digitilt Classic Inclinometer System - DGSI - Durham Geo - Inclinometers, (n.d.). https://durhamgeo.com/product/digitilt-classic-inclinometer-system/ (accessed December 16, 2020).

[16] A.D. Kersey, M.A. Davis, H.J. Patrick, M. LeBlanc, K.P. Koo, C.G. Askins, M.A. Putnam, E.J. Friebele, Fiber grating sensors, J. Lightwave Technol. 15 (1997) 1442–1462, http://dx.doi.org/10.1109/50.618377.

[17] F.W.D. Pfrimer, M. Koyama, A. Dante, E.C. Ferreira, J.A.S. Dias, A closed-loop interrogation technique for multi-point temperature measurement using Fiber bragg gratings, J. Lightwave Technol. 32 (2014) 971–977 http://jlt.osa.org/abstract.cfm?URI=jlt-32-5-971.

[18] B.-J. Peng, Y. Zhao, Y. Zhao, J. Yang, Tilt sensor with FBG technology and matched FBG demodulating method, IEEE Sens. J. 6 (2006) 63–66, http://dx.doi.org/10.1109/JSEN.2005.845198.

[19] H.-J. Chen, L. Wang, W.F. Liu, Temperature-insensitive fiber Bragg grating tilt sensor, Appl. Opt. 47 (2008) 556–560, http://dx.doi.org/10.1364/AO.47.000556.

[20] K. Ni, X. Dong, Y. Jin, H. Xu, Temperature-independent fiber bragg grating tilt sensor, Microw. Opt. Technol. Lett. 52 (2010) 2250–2252, http://dx.doi.org/10.1002/mop.25425.

[21] X. Dong, C. Zhan, K. Hu, P. Shum, C.C. Chan, Temperature-insensitive tilt sensor with strain-chirped fiber Bragg gratings, IEEE Photonics Technol. Lett. 17 (2005) 2394–2396, http://dx.doi.org/10.1109/LPT.2005.857978.

[22] H. Bao, X. Dong, C. Zhao, L.Y. Shao, C.C. Chan, P. Shum, Temperature-insensitive FBG tilt sensor with a large measurement range, Opt. Commun. 283 (2010) 968–970, http://dx.doi.org/10.1016/j.optcom.2009.11.014.

[23] H.Y. Au, S.K. Khijwania, H.Y. Fu, W.H. Chung, H.Y. Tam, Temperature-insensitive fiber bragg grating based Tilt sensor with large dynamic range, J. Lightwave Technol. 29 (2011) 1714–1720, http://dx.doi.org/10.1109/JLT.2011.2132695.

[24] S. He, X. Dong, K. Ni, Y. Jin, C.C. Chan, P. Shum, Temperature-insensitive 2D tilt sensor with three fiber bragg gratings, Meas. Sci. Technol. 21 (2010), http://dx.doi.org/10.1088/0957-0233/21/2/025203.

[25] H. Xu, F. Li, W. Zhao, S. Wang, Y. Du, C. Bian, A high precision fiber bragg grating inclination sensor for slope monitoring, J. Sens. 2019 (2019), http://dx.doi.org/10.1155/2019/1354029.

[26] C. Hong, Y. Zhang, Z. Lu, Z. Yin, A FBG tilt sensor fabricated using 3D printing technique for monitoring ground movement, IEEE Sens. J. 19 (2019) 6392–6399, http://dx.doi.org/10.1109/JSEN.2019.2908873.

[27] G. Yongxing, Z. Dongsheng, F. Jianjun, L. Shaobo, Z. Shengzhuo, Z. Fangdong, Development and operation of a fiber Bragg grating based online monitoring strategy for slope deformation, Sens. Rev. 35 (2015) 348–356, http://dx.doi.org/10.1108/SR-01-2015-0012.